Iridium Dihydroxybipyridine Complexes Show That Ligand Deprotonation Dramatically Speeds Rates of Catalytic Water Oxidation

Joseph DePasquale,[†,‡] Ismael Nieto,[†,‡] Lauren E. Reuther,[†] Corey J. Herbst-Gervasoni,[†] Jared J. Paul,*[,§] Vadym Mochalin,[⊥] Matthias Zeller,[∥] Christine M. Thomas,[¶] Anthony W. Addison,[†] and Elizabeth T. Papish*[,†]

[†]Department of Chemistry and [⊥]Department of Materials Science and Engineering, Drexel University, 3141 Chestnut Street, Philadelphia, Pennsylvania 19104, United States

[§]Department of Chemistry, Villanova University, 800 Lancaster Avenue, Villanova, Pennsylvania 19085, United States

[∥]Department of Chemistry, Youngstown State University, One University Plaza, Youngstown, Ohio 44555, United States

[¶]Department of Chemistry, Brandeis University, 415 South Street, Waltham, Massachusetts 02453, United States

S *Supporting Information*

ABSTRACT: We report highly active iridium precatalysts, $[Cp*Ir(N,N)Cl]Cl$ (**1−4**), for water oxidation that are supported by recently designed dihydroxybipyridine (dhbp) ligands. These ligands can readily be deprotonated in situ to alter the electronic properties at the metal; thus, these catalyst precursors have switchable properties that are pH-dependent. The pK_a values in water of the iridium complexes are 4.6(1) and 4.4(2) with (N,N) = 6,6′-dhbp and 4,4′-dhbp, respectively, as measured by UV−vis spectroscopy. For homogeneous water oxidation catalysis, the sacrificial oxidant $NaIO_4$ was found to be superior (relative to CAN) and allowed for catalysis to occur at higher pH values. With $NaIO_4$

as the oxidant at pH 5.6, water oxidation occurred most rapidly with (N,N) = 4,4′-dhbp, and activity decreased in the order 4,4′-dhbp (**3**) > 6,6′-dhbp (**2**) ≫ 4,4′-dimethoxybipyridine (**4**) > bipy (**1**). Furthermore, initial rate studies at pH 3−6 showed that the rate enhancement with dhbp complexes at high pH is due to ligand deprotonation rather than the pH alone accelerating water oxidation. Thus, the protic groups in dhbp improve the catalytic activity by tuning the complexes' electronic properties upon deprotonation. Mechanistic studies show that the rate law is first-order in an iridium precatalyst, and dynamic light scattering studies indicate that catalysis appears to be homogeneous. It appears that a higher pH facilitates oxidation of precatalysts **2** and **3** and their $[B(Ar^F)_4]^−$ salt analogues **5** and **6**. Both **2** and **5** were crystallographically characterized.
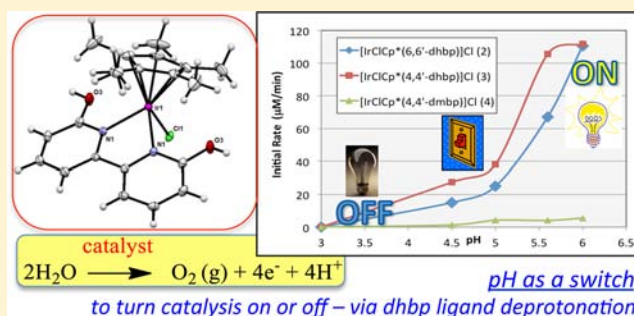
INTRODUCTION

Water oxidation is one of the most promising methods of harnessing and storing energy from the sun. Water oxidation forms oxygen, protons, and electrons (eq 1), and when this process is coupled with proton reduction, a clean and sustainable means of producing hydrogen as a fuel is realized.[1] Understanding the mechanistic details of water oxidation is critical for designing efficient catalysts. Synthetic water oxidation catalysts (WOCs) have commonly featured ruthenium,[2] iridium,[3,4] and manganese,[5] with rare usage of iron,[1,6,7] cobalt,[2,8−12] and recently copper.[3,4,13] The first-row transition metals are more readily available, but catalysts made from precious metals are often more active and can be sustainable if they are recycled. The intricate mechanistic details behind water oxidation are still not well understood, in particular concerning the role of hydrogen-bonding groups near the metal. Nature's WOC, the oxygen-evolving complex in photosystem II,[5,14] contains protic residues and water molecules near the active site that form hydrogen bonds and facilitate proton-coupled electron transfer (PCET).[9]

$$2H_2O \rightarrow O_2(g) + 4H^+ + 4e^- \qquad (1)$$
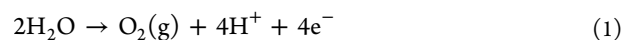
Hydrogen-bonding groups (on ligands) near the metal can potentially serve two purposes in reactions. They can interact with (metal-bound) substrates and supply or accept protons to facilitate proton shuttling steps[15] (also known as metal−ligand bifunctional catalysis, MLBC), or they can lead to pH-switchable catalysis, whereby ligand deprotonation events can change the amount of electron density at the metal and can switch a catalyst between "active" and "inactive" forms.[16,17] *We are not aware of any examples where WOCs switch on or off by*

simply changing the pH. In some cases, very active C−H bond activation catalysts have been formed by the addition of basic or acidic groups,[18] and this area has attracted a lot of recent attention.[19] The use of proton shuttling sites, acid/base-sensitive ligands, and MLBC has led to very active catalysts for certain transformations (e.g., hydrogenation[20]), but thus far this sort of approach is rare in water oxidation.[21,22]

Homogeneous iridium WOCs have been recently developed[4] and shown to be extraordinarily active.[3] Crabtree, Brudvig, et al. reported several iridium half-sandwich complexes as WOCs, including [Cp*Ir(bipy)Cl]$^+$ (**1**). These catalytic properties caught our attention because bipyridine (bipy) is ubiquitous in organometallic catalytic chemistry, but bipy has rarely been modified to be sensitive to protonation and deprotonation events in these catalysts. The introduction of basic N atoms has been done, including 2,2′-bipyrimidine complexes,[2,18] but the introduction of acidic groups is a more recent development.

Dihydroxybipyridine (dhbp; Scheme 1) ligands show promise for supporting catalysts and allowing acid/base-

Scheme 1. dhbp Ligands and Tautomers[a]
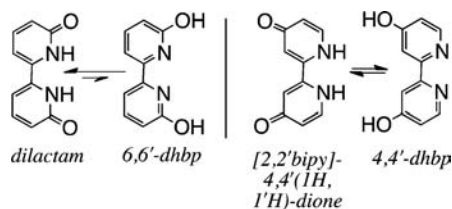
[a]The rotamers poised for metal binding are shown, but rotamers with the N atoms *s-trans* are likely favored prior to metal binding.

sensitive properties. With acidic OH groups in the 4 and 4′ positions, dhbp complexes of iridium, rhodium, and ruthenium are hydrogenation catalysts.[16,17] When deprotonated, these complexes are highly active for catalytic aqueous CO$_2$ hydrogenation because of enhanced ligand electron-donor properties, and under acidic conditions, the complexes become protonated, resulting in a change in the complex charge, decreasing activity, and solubility to facilitate catalyst removal by separation. Furthermore, Paul et al. have studied the same ligand in [(bipy)$_2$Ru(4,4′-dhbp)]$^{2+}$ complexes by UV−vis and cyclic voltammetry (CV) at varied pH and have shown that upon deprotonation the ligand has substantial C=O and N$^−$ character that alters the redox properties.[23] These changes are relevant to PCET, a key process in water oxidation.[24]

The Papish group[25] and two other groups[26,27] simultaneously developed the first 6,6′-dihydroxybipyridine (6,6′-dhbp) complexes as transition-metal catalysts. One advantage of this ligand is that the OH or O$^−$ groups are near the metal center, and this may lead to a MLBC mechanism, as seen computationally with 2-pyridinol/pyridinolate iridium catalysts for dehydrogenation.[28,29] Fujita and co-workers investigated various mono- and dihydroxybipyridine complexes of iridium as catalysts for acceptor-less dehydrogenation. They found that the 6,6′-dhbp complexes were more active than the 4,4′ derivatives, suggesting participation of the ortho basic O$^−$ groups (generated in situ) in the mechanism.[27] Similarly, Himeda and co-workers reported enhanced CO$_2$ hydrogenation with ortho basic groups;[30,31] this was published during the preparation of this manuscript. Because WOCs make use of PCET[2] (e.g., in transformations from Ir^{III}OH$_2$ to Ir^{IV}OH to Ir^V=O proposed for **1**),[3] we proposed that the presence of

basic groups on the ligands could aid catalysis. Two modes of rate enhancement are possible: (1) MLBC (when the O$^−$ groups are near the metal to assist in proton-transfer events) or (2) electronic tuning of the catalysts by deprotonation. Our goals included determining whether these two mechanistic possibilities (in concert or separately) enhanced catalytic rates of water oxidation by studying catalysts with different orientations of the hydroxyl groups.

■ RESULTS

Synthesis and Properties of dhbp Ligands. The synthesis and isolation of 6,6′-dhbp, which is the dilactam tautomer prior to complexation, have been previously reported (Scheme 1).[32] We prefer this synthesis to others in the literature[26,33] because it is efficient and avoids the use of F$_2$(g). Spectral data (IR, ν 1634 cm^{-1}; ^{13}C NMR, C=O at δ 165.8) suggest the presence of amide functional groups. However, the dilactam tautomer of 6,6′-dhbp is suitable for metal complex synthesis because tautomerization occurs readily in situ (see Schemes 1 and 2).[25]

Scheme 2. Preparation of Iridium Complexes 1−4
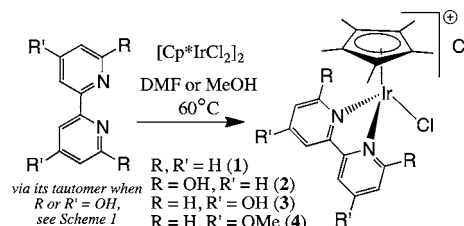
Design Criteria for and Synthesis of Metal Complexes. Our rationale in designing complexes for catalysis of water oxidation was to determine what role deprotonation and the location of the OH groups played in catalysis, in part by using methoxy groups on bipy as a control. In order to have a library of potential precatalysts with varied features, we prepared analogues of **1** that feature two OH groups ortho [[η^5-Cp*IrCl(6,6′-dhbp)]Cl (**2**)] or para (**3**) to the N atoms or OMe groups para to the N atoms (**4**) (Scheme 2). Complexes **1**,[3] **3**,[16] and **4**[16] are known in the literature, and our characterization data [^{1}H and ^{13}C NMR, IR, and mass spectrometry (MS)] matched these published procedures. Complex **2**, [Cp*IrCl(6,6′-dhbp)]Cl, is new (although closely related to the recently published[27] aqua analogue, [Cp*Ir-OH$_2$(6,6′-dhbp)]$^{2+}$) and was prepared by treating the dilactam form of 6,6′-dhbp (Scheme 1) with [Cp*IrCl$_2$]$_2$ in *N,N*-dimethylformamide (DMF) at 60 °C for 24 h. This complex was isolated in good yield (67%) as a bright-yellow solid that is air- and moisture-stable and was characterized by ^{1}H and ^{13}C NMR, IR, and MS (Figures SI-1−SI-4 in the Supporting Information, SI). Recrystallization of **2** from saturated methanol (MeOH) gave blocks suitable for single-crystal X-ray crystallography for structure determination (Figure 1 and the SI). Complexes **2** and **3** have also been prepared from MeOH, with similar yields and characterization data.

In the course of our CV studies (described below), it became necessary to have derivatives of **2** and **3** with improved solubility in organic solvents. We prepared [Cp*IrCl(6,6′-dhbp)]B(Ar^F)$_4$ [**5**, where Ar^F = 3,5-(CF$_3$)$_2$-phenyl] in 88% yield from **2** via a salt metathesis route with NaB(Ar^F)$_4$. Complex **5** crystallized from CH$_2$Cl$_2$ and hexanes as yellow
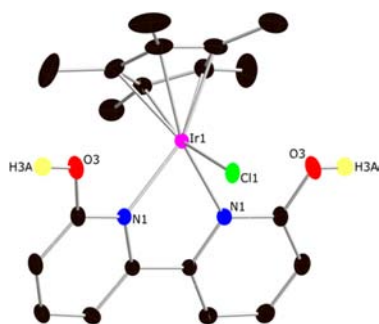
Figure 1. Molecular structure of **2**. The counteranion and H atoms (except in OH groups) are removed for clarity, and ellipsoids are shown at 50% probability. Selected bond lengths (Å) and angles (deg): Ir1−N1 = 2.103(14), Ir1−Cl1 = 2.415(7), Ir−C$_5$(Cp*) = 2.165(1) (avg); N1−Ir1−N1 = 75.92 (8), Cl1−Ir1−N1 = 86.46(4).

blocks, and its structure is described below (Figure 2). Complex **6**,[Cp*IrCl(4,4′-dhbp)]B(Ar^F)$_4$, was prepared similarly from **3**, as described in the Experimental Section.
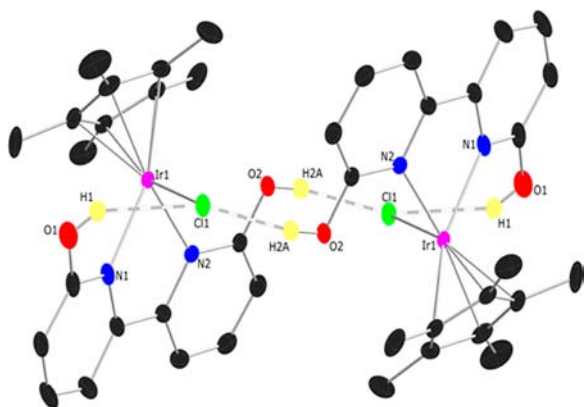
Figure 2. Molecular structure of **5**. The counteranion and H atoms (except in OH groups) are removed for clarity, and ellipsoids are shown at 50% probability. Selected bond lengths (Å) and angles (deg): Ir1−N1 = 2.101(2), Ir1−N2 = 2.110(2), Ir1−Cl1 = 2.4148(3), Ir−C$_5$(Cp*) = 2.158(1) (avg), O1−Cl1 (nonbonded but provide a measure of hydrogen bonding) = 3.306(1), O2−Cl1 = 3.092(1); N1−Ir1−N1 = 75.67(6), Cl1−Ir1−N1 = 84.97(4), Cl1−Ir1−N1 = 91.79(4).

Crystal Structures of Complexes 2 and 5. For both complexes, a piano-stool geometry is observed with bond lengths [Ir−Cl, Ir−N and Ir−C$_5$(centroid)] and angles (see Figures 1 and 2) that are similar to those of structurally related iridium bipyridine analogues and ruthenium dihydroxybipyridine complexes.[25] The OH groups within the dhbp ligand are intact and do not participate in metal binding (O···Ir = ~3.2 Å). However, in **2**, there are OH···Cl hydrogen bonds [with the noncoordinated chloride, O3···Cl2 = 2.988(1) Å], which lead to structured packing arrangements with a two-dimensional network of hydrogen bonds [see Figure SI-7 in the SI; H3A···Cl2 = 2.1604(7) Å and O3−H3A···Cl2 = 168.41(9)°].

The structure of **5** is very similar to that of **2** but differs in the placement of hydrogen bonds. Without the chloride counteranion, OH···Cl hydrogen bonds now utilize the iridium-bound chloride and form a dimer of **5** (Figure 2). The O···Cl distances of ~3.09 and 3.31 Å respectively are consistent with a hydrogen bond and a weak interaction [H···Cl distances are 2.2598(4) and 2.5667(4) Å].[34] Similarly, a more linear O−H···Cl angle

indicates a stronger interaction,[34] and here the angles are 170.91(9) and 147.4(1)°, respectively.

While hydrogen bonding in **2** is similar to that seen with [(η^6-arene)Ru(6,6′-dhbp)Cl]Cl complexes,[25] complex **5** is unique in that it shows how the OH groups can be angled toward the chloride ligand and potentially poised to hydrogen bond with substrates. The bond lengths and angles are such that a deprotonated ligand would have an O$^-$ group in close proximity to an OH$_2$ or OH group on iridium and could potentially assist in proton-transfer events.

Acidity of the Iridium Complexes. By obtaining UV−vis spectra for **2** (Figure 3) and **3** at varied pH values in water (pH
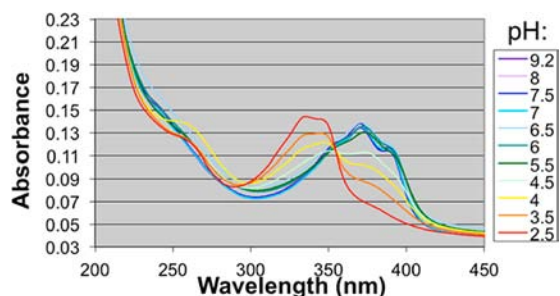
Figure 3. UV−vis spectra of **2** as a function of the pH. The legend shows the pH values. This method was used to establish an average pK_a value for **2** of 4.6 ± 0.1 from two experiments (see the SI for further details).

kept constant with a phosphate buffer and a constant concentration of **2** or **3**), we were able to determine that the pK_a values are 4.6 ± 0.1 and 4.4 ± 0.2 for **2** and **3**, respectively (see the SI for details). It appears that metal complexation lowers the pK_a values of dhbp ligands by several orders of magnitude (see the SI for approximate ligand pK_a values), as expected.[35,36]

It needs to be noted that the pK_a value (4.4) that we report for **3** differs considerably from the value reported by Himeda (9.6).[17] Himeda's data for pH-dependent UV−vis spectra of **3** can be reinterpreted to give 4.8 as a revised pK_a value, and this value is roughly consistent with our value of 4.4 (see the SI).

Also noteworthy is the observation, for both **2** and **3**, that two protons are removed in rapid succession because we see only one inflection point by plotting the absorbance versus pH at a single wavelength (see Figure SI-12 in the SI). This suggests that the two protons on each dhbp ligand have nearly the same pK_a value. However, close inspection of Figure 3 shows that the isosbestic point is not well-defined, and so there appears to be some monodeprotonated dhbp present (perhaps assignable to the small bump at ~260 nm in studies of **2**) prior to formation of the doubly deprotonated species. Similar observations (of nearly simultaneous double deprotonation) were made by Paul et al.[23] for [(bipy)$_2$Ru(4,4′-dhbp)]$^{2+}$, by Himeda for **3**,[17] and by us for [(η^6-arene)Ru(6,6′-dhbp)Cl]-Cl.[25]

Complex **2** is doubly deprotonated at neutral pH, and this complex shows an intense ligand-to-metal charge-transfer (LMCT) band at λ = 375 nm and ε = 16,100 M^{-1} cm^{-1}. Similarly, we report for doubly deprotonated **3** LMCT band values of λ = 251 nm and ε = 27900 M^{-1} cm^{-1} (Figure SI-14 in the SI). The bands for **2** and **3** both shift to shorter wavelengths (higher energy) upon protonation (to 336 and 230 nm, for **2** and **3**, respectively). This trend makes sense because doubly

deprotonated dhbp is dianionic and more electron-rich, resulting in a higher-energy, predominantly ligand-based highest occupied molecular orbital. Further analysis may be needed to understand why for both forms of **2** charge-transfer transitions are more energetically accessible than those in **3**.

We can confirm that these pH-sensitive spectroscopic features are due to ligand deprotonation events rather than Ir—OH₂ (formed from Ir—Cl) deprotonation. UV–vis spectra of **1** (the bipy complex that lacks a protic ligand) at constant concentration were monitored as a function of the pH (Figure SI-15 in the SI). No isosbestic points were observed from pH 2 to 7.8. Only at pH 9 did we see a change in the spectral features, suggesting that (at least in the absence of oxidation events) Ir—Cl is not replaced by Ir—OH until high pH.

Water Oxidation Catalysis. Our first goal for water oxidation catalysis was to find conditions that gave optimal rates of oxygen formation with the dhbp complexes of iridium. We began optimization of the conditions with complex **2**, which was prepared first. The initial conditions in which cerium(IV) ammonium nitrate (CAN) was used as the sacrificial oxidant gave both qualitative and quantitative evidence of oxygen formation.[3] Oxygen formation was first observed by combining aqueous solutions of **2** and CAN in a sealed vessel under an inert (N₂) atmosphere. Bubbles were noticed and oxygen formation was confirmed by headspace gas chromatography–mass spectrometry (GC–MS) analysis,[37] and in the absence of complex **2**, no oxygen was detected (see Figures SI-16 and SI-17 in the SI for details). However, in terms of monitoring the evolution of oxygen with time, the GC–MS analysis method proved too prone to error for quantitative rate data.

Rate data for water oxidation are most easily measured by the use of a Clark-type electrode to detect dissolved oxygen (DO) via a polarographic probe (Figure SI-18 in the SI). Upon the addition of a precatalyst (**2**) to CAN in water (at 25 °C in a water-jacketed vessel, with final concentrations of 5 μM **2** and 78 mM CAN at pH 0.6), oxygen evolution begins immediately (Figure SI-19 in the SI). Similar experiments were done with **3**, by us and very recently by others,[38] and studies of **1** are in the literature at the same concentrations of precatalyst and oxidant.[3] As shown in Table 1, **2** and **3** perform similarly to

Table 1. Rates of Iridium-Catalyzed Oxygen Evolution with CAN as the Primary Oxidant

precatalyst	initial rate (μM min⁻¹)[a]	TOF (min⁻¹)[b]
2	75 ± 15	15 ± 15
3	81 ± 12	16 ± 12
1[c]	72 ± 3	14.4 ± 0.7

[a]Measured by Clark-type electrode oxygen assays. Errors (±n) were calculated from the standard deviation of three measurements. The initial rates are from the first 30 s. Conditions: 5.0 (±0.1) μM precatalyst; 78 mM CAN (pH < 1); 25 °C. [b]TOFs are initial rate/(μM Ir). [c]Values from the literature[3] and reproduced in our laboratory.

or slightly better than **1** in terms of the initial rates and turnover frequency (TOF) values, *at this particular pH*. For these studies, the pH must be below 1 because CAN is only stable and soluble at low pH. Thus, **2** and **3** are most likely protonated under these conditions (some uncertainty is introduced because the pK_a values of oxidized **2** and **3** are unknown but presumably lower), and we hypothesized that raising the pH

would change the catalytic properties of **2** and **3** via ligand deprotonation.

Furthermore, recent reports have called attention to the fact that CAN oxidizes many organic ligands,[39] and so there is some debate in the literature as to whether iridium precatalysts that use CAN are really homogeneous WOCs or heterogeneous[40] catalyst materials including perhaps thin films[41] or nanoparticles (NPs) made of IrO$_x$ or an Ir–Ce agglomeration, with characteristic UV–vis spectra reported.[42] (Similarly, some cobalt homogeneous water oxidation precatalysts form NPs as the active catalysts.[43−45]) Indeed, we did observe a slight discoloration of our solutions (see UV–vis spectra, at elevated concentrations of CAN and iridium precatalysts; Figure SI-23 in the SI) when oxidizing water with CAN and **2**. However, the absorbance at ~560 nm in the UV–vis spectrum could alternatively be an iridium(IV) species, as described by Crabtree, Brudvig, et al.[46,47] Furthermore, rate data were not consistent run-to-run. Another downside to low pH is the highly corrosive conditions that can eventually damage the DO probe. Thus, for many reasons, we sought oxidants that would allow the use of near-neutral-pH solutions, as would be required for large-scale practical applications of water oxidation.

In order to pursue higher pH studies, an alternate sacrificial oxidant was needed. Recently, a report by Crabtree, Brudvig, et al. used sodium periodate (NaIO₄) as the sacrificial oxidant for water oxidation with an iridium acetate trimer as the catalyst in aqueous solutions buffered at pH 5.6 with NaOAc.[46,47] By using Crabtree's conditions (20 mM NaIO₄, 180 mM NaOAc buffer, pH 5.6), we were able to oxidize water with 5 μM **2** or **3** as the precatalyst, and we observed excellent run-to-run consistency. Water oxidation begins immediately after the precatalyst is introduced to the oxidant solution; i.e., no lag time is observed. This observation suggests that complexes **2−4** form homogeneous catalysts with NaIO₄ as the oxidant rather than precursors to a heterogeneous species. Unlike with CAN (above and in ref 42), with periodate no visible discoloration of the aqueous solutions was observed. Following the work of Crabtree, Brudvig, et al.,[47] we used dynamic light scattering (DLS) to check on the possible presence of NPs in the solution. It should be noted here that DLS is not a detection technique and therefore cannot measure the NPs if their concentration is not high enough. Moreover, even if the concentration is high enough, the technique cannot reliably measure particles whose size are <1 nm, although it has been shown that in ideal conditions it is possible to measure the size of subnanometer particles with DLS.[48] DLS for a solution of **2** or **3** at 136 μM showed no evidence of NP formation over 20 min (with 10 mM NaIO₄ and pH 6, 180 mM acetate buffer present for consistency; see the SI). At the same time, a control experiment confirmed that NPs are detected when a solution known to form NPs[47] is used (IrCl₃ at 136 μM; see the SI). Therefore, we conclude with confidence that in the system containing periodate there are no NPs larger than 1 nm in concentrations high enough to be detected by DLS. An explanation for the lack of NP formation with periodate is that it is a less potent oxidizing agent than CAN (equivalent to an overpotential of ~0.42 vs 1.7 V provided by CAN)[47] and is therefore less likely to oxidize organic ligands (including Cp*[42,47] and 6,6′ or 4,4′-dhbp[49,50]), and ligand oxidation is believed to be a key step in forming heterogeneous materials from iridium catalyst precursors.[42]

Rates of water oxidation with periodate do not appear to depend on the oxidant concentration as long as sufficient (>10

mM) oxidant is used (see the SI and discussion below under mechanistic studies). No oxygen evolution occurs prior to the addition of an iridium precatalyst; this suggests that $NaIO_4$ decomposition is not a source of oxygen. Isotopic labeling studies with O-labeled water were not pursued because of rapid O-atom exchange between periodate and water.[51] However, when **2** is combined with periodate in thoroughly dried MeOH, no oxygen is formed; this suggests that water is necessary for oxygen formation and iridium precatalysts do not catalyze decomposition of periodate. Thus, the combined evidence including control experiments, water oxidation with iridium precatalysts, and two different oxidants (CAN and $NaIO_4$) and studies in the literature[47] suggest that sodium periodate here acts as an oxidant rather than a source of oxygen.

Water oxidation catalysis was investigated with **2** and **3** to determine the impact of hydroxyl groups and their protonation state and with **4** to determine the impact of neutral O-atom donors, versus **1** as a control. We were intrigued by the fact that, under periodate conditions at pH 5.6, **2** and **3** are much more active for water oxidation than **1**, with rates 156 and 185 times greater, respectively (see Table 2). Figure 4 shows oxygen

Table 2. Rates of Iridium-Catalyzed Oxygen Evolution with $NaIO_4$ as the Primary Oxidant

catalyst	initial rate $(\mu M\ min^{-1})^a$	initial TOF $(min^{-1})^b$	TOF $(min^{-1})^c$	TON at 10 min
1	0 ± 3	0 ± 3	0.064	0.64
2	50 ± 3	10 ± 3	10	100
3	106 ± 3	21 ± 3	12	120
4	0 ± 3	0 ± 3	0.67	6.7

^{a}Measured by Clark-type electrode oxygen assay; triplicate data sets were collected for each rate measurement. Errors (presented as $\pm n$) were calculated from the accuracy of the DO meter recording the measurement. The initial rates are from the first 30 s. Conditions: $5.0(\pm0.1)\ \mu M$ precatalyst; 20 mM $NaIO_4$; 180 mM NaOAc buffer (pH 5.6); 25 °C. ^{b}TOFs are initial rate/(μM Ir). ^{c}Calculated as in footnote b after 10 min.
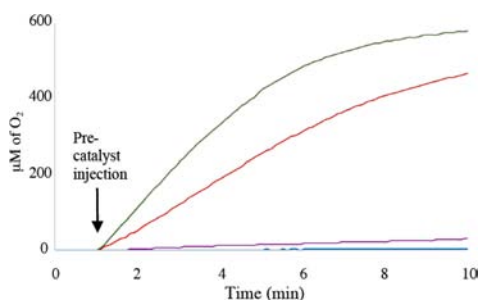
Figure 4. Water oxidation as measured by oxygen evolution with precatalysts **1**−**4** and $NaIO_4$ as the oxidant. Color code: **1**, blue; **2**, red; **3**, green; **4**, purple. Conditions: 5 (±0.1) μM precatalyst, 20 mM $NaIO_4$ in 180 mM NaOAc buffer (pH 5.6) at 25 °C.

evolution as a function of time for complexes **1**−**4** using $NaIO_4$ at pH 5.6. It is clear that, with lower concentration of a weaker oxidant (relative to CAN studies[3]), precatalyst **1** is inactive with a rate of zero (within experimental error; Table 2), despite this precatalyst being active with CAN (Table 1). Perhaps periodate does not oxidize **1** to form an active catalyst because it is a less potent oxidant and is necessarily at lower concentration because of solubility. However, complexes **2** and **3** are excellent WOCs at this pH with initial rates of 50 and 106 $\mu M\ min^{-1}$,

respectively [see Table 2 for rates, TOFs, and turnover numbers (TONs)]. For complex **3**, catalysis with periodate is much faster than that with CAN, and this appears to be a pH effect. Precatalyst **4** with methoxy groups is sluggish and only slightly faster than **1**. Thus, ligand deprotonation with **2** and **3**, presumably to enhance donicity, appears to be essential for fast catalysis, and methoxy groups alone are not strong enough donors. Complex **3**, with OH groups para to N, is the most active precatalyst at this pH; thus, it appears that OH groups need not be near the metal center. The enhanced donicity in deprotonated OH groups may facilitate oxidation of the precatalyst to yield a high-valent Ir^V=O species, which has been proposed in other mechanistic studies[3] (also see the Electrochemistry section).

Furthermore, because the pK_a values for **2** and **3** are both 4.6 and 4.4, respectively (see above), by adjustment of the pH of the reaction environment, **2** and **3** should show dramatic changes in activity. Indeed, Figure 5 shows that precatalysts
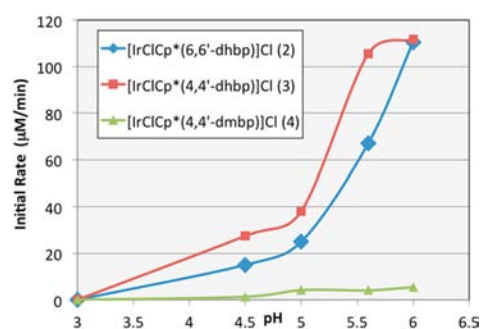
Figure 5. Initial rate of oxygen production ($\mu M\ min^{-1}$) versus pH as measured during time = 30−240 s.

2−**4** are all inactive WOCs at pH 3 with periodate as the oxidant (Table 3). However, with increasing pH, precatalysts **2**

Table 3. Initial Rates of Oxygen Evolution with Precatalysts 2−4 Depending on the pH

pH	initial rate $(\mu M\ min^{-1})^a$		
	2	3	4
3	0	0	0
4.5	15	27	1.3
5	25	38	4.2
5.6	67	106	4.1
6	110	112	5.5

^{a}Measured by Clark-type electrode oxygen assay for 10 min. Data for initial rates of 30−240 s. Conditions: 5.0 (±0.1) μM precatalyst; 20 mM $NaIO_4$ in a 180 mM NaOAc buffer. Vessel and precatalyst solution maintained at 25 °C.

and **3** improve activity over 100-fold, and precatalyst **4** shows only modest increases in activity (∼5-fold). It is well studied in the literature that water oxidation is always faster at higher pH,[13,52,53] given that high pH results in a greater concentration of hydroxide, which is easier to oxidize than water. For this reason, we wanted to confirm that the increase in the water oxidation rates is due to ligand deprotonation rather than the effect of the pH alone.

The enhancement in rate with the pH in Figure 5 resembles a titration curve and shows that ligand deprotonation is likely responsible for over 95% of the rate increase. It is worth noting

that the inflection points in the curves in Figure 5 occur at pH ~5.3 for precatalyst **3** and at pH ~5.5 for precatalyst **2**; this mirrors the fact that the pK_a values for **3** and **2** are 0.2 units apart and **3** is more acidic. It is not clear why this rise occurs at higher pH than the apparent pK_a value; however, it may be that we see "averaged" pK_a values at 4.6 and 4.4 for the removal of both protons, and likely the true pK_a for removal of the second proton is higher. A plausible explanation is that the removal of both protons is needed for ease of oxidation to form the active species, and both protons are not removed until well above pH 5. The curve for precatalyst **2** was still rising at pH 6, but the acetate buffer does not support pH values higher than 6. It is unknown whether precatalyst **2** at pH above 6 would show rates of water oxidation that level off or surpass **3** under these conditions.

These data indicate that complexes **2** and **3** are inherently much more active for water oxidation when they are deprotonated at pH 6. *This result demonstrates the ability to use pH as a switch to turn catalysis on or off, and to the best of our knowledge, this feature is unprecedented for water oxidation catalysis.*

Mechanistic Studies. We have done a preliminary investigation of the rate law of water oxidation with **2**, which is a very active precatalyst and a novel species in the literature. As shown in Figure 6, the rate of water oxidation is dependent
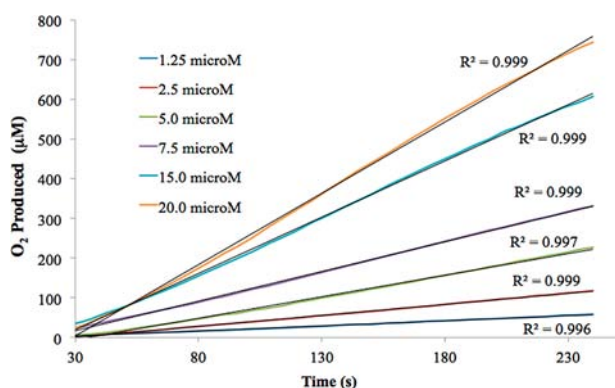
Figure 6. Rate of water oxidation plotted as a function of the concentration of the precatalyst **2** (in the legend) with 17 mM NaIO$_4$ at 25 °C. Colored lines represent data, and black lines are fit with the R^2 value listed. For rate data at each concentration, see Table SI-12 in the SI.

on the concentration of **2**. Rates are most linear from 30 to 240 s, and this region was used for analysis because mixing is not complete within 0−30 s and oxygen diffusion into the headspace (which cannot be detected by the DO meter) causes inaccuracies at longer times (this problem is also discussed in the literature).[42] The rate law is clearly first-order in **2**, with a plot of rate versus concentration giving a visibly linear trend with R^2 = 0.997. Furthermore, a plot of ln(rate) vs ln([**2**]) is linear with slope = 0.94; in this analysis, the slope corresponds to the reaction order. See the SI for plots (Figures SI-27 and SI-28 and Table SI-12) and further details. Thus, it seems likely that a monomeric species (derived from **2** by perhaps oxidation or formation of an aqua complex) catalyzes water oxidation. Electrochemistry experiments relevant to the formation of oxidized species are described below.

The concentration of the oxidant does not appear to have a significant impact on the rate with **2**, as long as the oxidant concentration is at least 10 mM (Figure SI-29 in the SI). A

similar trend was reported in the literature: the iridium acetate trimer shows rates with a first-order dependence on NaIO$_4$ at low (<5 mM) concentration, but this trend levels off at 5−10 mM because of saturation kinetics.[46] Presumably above 10 mM there is an ample quantity of oxidant to oxidize **2** to yield the active species and absorb electrons generated by water oxidation, as shown in eq 1 (5 μM **2** and 17 mM oxidant represents a 3400-fold excess).

The kinetic isotope effect (KIE) for water oxidation done with D$_2$O rather than H$_2$O shows k_H/k_D = 1.118. The relatively small isotope effect suggests that proton removal is not the rate-determining step. A similar KIE was observed with **1** in a high concentration of the oxidant regime (KIE = 1.15), while the KIE was inverse (0.65) at a low concentration of oxidant (insufficient oxidant for water oxidation).[3] This study[3] and others have suggested that iridium oxidation may be the slow step in water oxidation,[47] and the combined evidence suggests a similar slow step in our case. A deprotonated ligand with enhanced donor ability (in **2** or **3**) should facilitate iridium oxidation.

Electrochemistry. We wished to perform CV experiments on complex **2** in an organic solvent, so that the oxidation of **2** could be observed without simultaneous catalytic water oxidation waves (which may complicate the interpretation). However, **2** would not dissolve in organic solvents at concentrations sufficient for analysis. Thus, **5**, the [B(Ar^F)$_4$]$^−$ analogue of **2**, was prepared for improved solubility. Complex **5** dissolves readily in dichloromethane and acetonitrile. CV in acetonitrile with [Bu$_4$N][PF$_6$] as the electrolyte showed that complex **5** has an irreversible oxidation at 1.53 V vs SCE. Upon the addition of 3 equiv of base as [Bu$_4$N]OH to a solution of **5** and electrolyte, we see a peak that we assign to irreversible oxidation of doubly deprotonated **5** at 0.50 V. There is also a large peak at 0.92 V that is base oxidation, as assigned from CV on the base and the electrolyte alone (a small shift is expected based upon **5** catalyzing base oxidation). The base oxidation peak is large and could potentially obscure other peaks; thus, only one oxidation event is evident for **5**.

Similarly, we prepared **6**, the [B(Ar^F)$_4$]$^−$ analog of **3**, and showed that the complex oxidizes irreversibly at 1.63 V vs SCE (same conditions as above). Upon the addition of the same base, [Bu$_4$N]OH, an irreversible oxidation can be assigned to deprotonated complex **6**, at ~0.6 V, although this assignment is uncertain because of overlap with base oxidation peaks.

It appears that doubly deprotonating the ligand in **5** or **6** shifts the oxidation of iridium by ~1.0 V in each case, and this can explain why the pH has such a dramatic influence on water oxidation catalysis. Similarly, others have observed that chelating LX-type ligands (e.g., phenylpyridine) make for more active WOCs than L$_2$-type ligands (e.g., bipyridine)[3] in [Cp*Ir(chelator)Cl]$^{n+}$ complexes (n = 0 or 1) because of more accessible oxidation in the former case.[54] However, what is remarkable in our study is that the type of ligand can be converted from L$_2$ to LX to X$_2$ in situ and reversibly.

■ DISCUSSION

Further mechanistic studies are ongoing in our laboratory, but the results presented thus far show that, with periodate as the oxidant, catalysis appears to be homogeneous with both **2** and **3**. The idea of O$^−$ groups near the metal assisting in and accelerating proton-transfer events is still possible, given that with **2** deprotonation may not have been complete at pH 6 (because the curve in Figure 5 is still rising at pH 6). A

mechanism that utilizes carboxylate-containing ligands for proton shuttling has been demonstrated for ruthenium WOCs.[21,22] However, from pH 4.5 to 5.6, this mode of rate enhancement has not been demonstrated for these iridium complexes because **3** (*p*-hydroxyls) is more active than **2** (*o*-hydroxyls). Thus, further studies will be needed to determine whether OH/O⁻ groups near the metal center play a role in proton transfer in water oxidation catalysis. The enhanced catalysis with **3** (vs **2**) contrasts with hydrogen-transfer reactions catalyzed by various $[Cp^*Ir(dhbp)OH_2]^{2+}$ and related complexes, whereby *o*-hydroxyls gave the most active catalysts[27,30,31] and these results suggest an MLBC mechanism with proton transfer involving the OH/O⁻ groups of the ligand. The hydroxyls in **2** and **3** appear to give their influence primarily through enhanced electron donation via resonance once deprotonated, but MLBC may still contribute to a lesser extent.

CONCLUSIONS

In conclusion, dhbp complexes of iridium are highly active for homogeneous catalytic water oxidation, and these precatalysts function best in relatively mild conditions including near-neutral pH with less oxidizing reagents. It is believed that dhbp's OH groups are doubly deprotonated at near-neutral-pH values, causing increased electron-donating character and heightened catalytic activity. This amounts to tuning of the catalytic properties *quickly*, *dramatically*, and *reversibly*. Other examples are known of catalysts switching activity and solubility with the pH, but this is the first time pH-switchable catalysis has been used to enhance water oxidation. Furthermore, this new precatalyst framework offers insight into how hydrogen bonds and acid/base-sensitive groups oriented near and far from the metal center can impact organometallic catalysis. These features and pH-dependent solubility properties[17] can enable green chemistry applications based upon water oxidation with dhbp-based catalysts.

EXPERIMENTAL SECTION

General Procedures. All experiments concerning the synthesis of iridium precatalysts were carried out in an inert atmosphere using standard Schlenk-line and/or glovebox techniques. The following ligands and complexes were prepared according to previously published methods:[16,17,32,55] 6,6′-dihydroxy-2,2′-bipyridine (6′,6-dhbp), 4,4′-dihydroxy-2,2′-bipyridine (4,4′-dhbp), 4,4′-dimethoxy-2,2′-bipyridine (4,4′-dmbp), $[Cp^*IrCl(4,4′-dhbp)]Cl$, $[Cp^*IrCl(4,4′-dmbp)]Cl$, and $[Cp^*IrCl(bipy)]Cl$. *N*,*N*-dimethylformamide (DMF) was dried by distillation of a MgSO₄/solvent mixture under N₂; distilled DMF was then stored in a glovebox in a Schlenk tube prior to use. MeOH was dried by distillation of a CaH₂/solvent mixture, followed by degassing of the solvent by freeze-pump-thaw and storage in a glovebox prior to use. Oxidants cerium(IV) ammonium nitrate (CAN) and sodium periodate (NaIO₄) were stored in a desiccator. Distilled, deionized, and purified water was obtained from a Millipore system. All other reagents were commercially available and were used without further purification. Glassware was dried in a 100 °C oven for 24 h prior to use. NMR spectra were recorded using either a 300 or 500 MHz Varian Unity Inova NMR spectrophotometer. Elemental analyses were performed by Robertson Microlit, Madison, NJ. IR spectra were recorded on a Perkin-Elmer Spectrum One Fourier transform infrared absorption spectrophotometer. High-resolution MS (HRMS) was performed on a VG70SE double-focusing, triple-quadrupole mass spectrometer equipped with fast-atom-bombardment or chemical-ionization capability. UV−vis spectra were recorded on a Perkin-Elmer Lambda 35 UV−vis spectrometer equipped with a Peltier constant-temperature bath.

Synthesis of $[Cp^*IrCl(6,6′-dhbp)]Cl$ (2). In a glovebox, 6,6′-dhbp (100 mg, 531 μmol), $[Cp^*IrCl_2]_2$ (211 mg, 266 μmol), and 10 mL of dry DMF were combined in a Schlenk flask. The reaction mixture appeared as a yellow-orange slurry; the flask was sealed, removed from the glovebox, and placed under N₂. The reaction was heated to 60 °C for 1 day. A bright-yellow solution resulted, and DMF was removed by vacuum distillation. The residue remaining was dissolved in minimal MeOH, and then copious amounts of Et₂O were added to precipitate out the product. The precipitant was isolated by filtration, washed with more Et₂O, and dried under vacuum, and this yielded 205 mg of product (65% yield). This complex can also be prepared by a similar procedure using MeOH as a solvent, to obtain a similar yield. ¹H NMR (DMSO-d_6): δ 13.30 (2H, OH), 7.98 (d, 4H, dhbp), 7.16 (t, 2H, dhbp), 1.55 (15H, Cp*). ¹³C NMR (DMSO-d_6): δ 163.96, 153.94, 141.73, 114.57, 113.06, 88.00, 9.38. IR (ν, cm⁻¹): 2854 (br), 1606 (C≡N ring mode), 1484 (ring mode), 1435, 1368, 1322, 1307, 1137, 1025, 821, 765, 717. HRMS. Calcd for cation of $[2 − Cl]^+$: m/z 551.107748. Found: m/z 551.109437 (error is 3.1 ppm). The isotopic pattern matched the predicted pattern based on isotopic modeling. See NMR, IR, and HRMS spectra and assignments for NMR resonances in Figure SI-1−SI-4 in the SI.

Synthesis of $[Cp^*IrCl(6,6′-dhbp)][B(Ar^F)_4]$ (5), Where $B(Ar^F)_4$ = Tetrakis[3,5-bis(trifluoromethyl)phenyl]borate. Complex **2** (10 mg, 0.017 mmol) and sodium tetrakis[3,5-bis(trifluoromethyl)-phenyl]borate (18 mg, 0.020 mmol) were dissolved in 0.5 mL of dichloromethane. To this solution was added 0.5 mL of deionized water, and the resulting solution was stirred for 12 h. The dichloromethane layer was removed from the aqueous layer, which was extracted three more times with 0.5 mL of dichloromethane. The combined organic solutions were dried with MgSO₄ and filtered, and the solvent was removed to produce a yellow solid (21 mg, 0.015 mmol, 87% yield). Crystals were obtained via the slow evaporation of 3:1 (by volume) dichloromethane and hexanes. ¹H NMR (CD₂Cl₂): δ 8.056−8.025 (t, 2H, dhbp), 7.848 (s, 2H, dhbp), 7.715 (s, 8H, B(Ar^F)₄), 7.554 (s, 4H, B(Ar^F)₄), 7.265−7.249 (d, 2H, dhbp), 1.593 (s, 15H, Cp*).

Synthesis of $[Cp^*IrCl(4,4′-dhbp)][B(Ar^F)_4]$ (6). Complex **6** was synthesized in a similar manner as that described above for the synthesis of **5**. Complex **3** (40 mg, 0.068 mmol) and sodium tetrakis[3,5-bis(trifluoromethyl)phenyl]borate (73 mg, 0.082 mmol) were stirred in a mixture of dichloromethane (2.0 mL) and deionized water (2.0 mL). This solution was allowed to mix for 1.5 h. Compound **6** was isolated as a yellow solid (96 mg, 0.068 mmol, 99% yield). ¹H NMR (DMSO): δ 12.10 (b, 2H, OH), 8.58 (d, 2H, dhbp), 7.90 (d, 2H, dhbp), 7.71 (s, 4H, B(Ar^F)₄), 7.61 (s, 8H, (B(Ar^F)₄), 7.19 (m, 2H, dhbp), 1.61 (s, 15H, Cp*).

Initial Rate Studies. The initial oxygen evolution rate studies were performed in a sealed jacketed reaction vessel, as shown in Figure SI-18 in the SI. Measurements of the initial oxygen evolution rate were made with a YSI Clark-type (polarographic probe, Y605203) DO probe connected to a YSI Professional Plus Meter. Prior to the beginning of each set of experiments, the gas-permeable membrane of the probe was replaced and the probe was calibrated. The DO probe, secured in a 25 mm threaded bushing, was then inserted into a tight-fitting water-jacketed glass vessel containing an oxidant solution (7 mL volume) and stir bar. The system and precatalyst stock solution were kept at a constant temperature of 25 °C, and the oxidant solution was stirred at 650 rpm. A GC septum (Therm Lb2, 11 mm diameter) was inserted into the septum-sealed cap, and the cap was sealed tightly.

In a typical CAN experiment, a freshly prepared CAN solution in Milli-Q water (7 mL, 91.4 mM, pH < 1) was added during the preparation of the system and allowed to equilibrate for 30 min. Data collection over 5 min showed equilibration of the system, and when a steady baseline was achieved, 1.2 mL of a precatalyst stock solution (34 μM **1** in Milli-Q water) was injected. Oxygen evolution commenced immediately and typically reached maximum evolution within 10 min of injection. Oxygen evolution data were recorded with YSI data manager software, and DO trace plots were fitted from raw data of concentration of oxygen versus time with oxidant and

precatalyst components reported as final concentrations after mixing for each (20 mM and 5.0 ± 0.1 μM).

In a typical NaIO$_4$ experiment, a freshly prepared NaIO$_4$ solution in a NaOAc buffer (7 mL, 23.4 mM, pH 5.6) was added during the preparation of the system and allowed to equilibrate for 30 min. A NaOAc buffer (180 mM, pH 5.6) was prepared in Milli-Q water and pH-tested for consistency prior to use. As noted in the CAN experiment, the system was equilibrated and monitored for a steady baseline in a same fashion. Once a steady baseline was achieved, 1.2 mL of a precatalyst stock solution (34 μM precatalyst in Milli-Q water) was injected. Oxygen evolution commenced immediately and typically reached the maximum value for the system within 30 min of injection. Oxygen evolution data were recorded with YSI data manager software, and DO trace plots were fitted from raw data of concentration of oxygen versus time with oxidant and precatalyst components reported as final concentrations after mixing for each (78 mM and 5.0 ± 0.1 μM) at the noted pH.

Computational Details. Computations were performed using *Gaussian09*[56] for the Linux operating system. Density functional theory calculations were carried out using the B3LYP hybrid functional, including Becke's parameter exchange functional (B3)[57] and the correlation functional of Lee, Yang, and Parr (LYP).[58] For the 4,4′-dhbp and 6,6′-dhbp ligands and their deprotonated derivatives, the 6-31G** basis set was used for all atoms.[59] For the iridium complexes **2** and **3** and their deprotonated derivatives, the 6-31G(d,p) basis set was used for C, H, O, N, and Cl atoms, while the Stuttgart/Dresden basis set with associated relativistic effective core potentials was used for the Ir atom.[60] All geometries were fully optimized using the SMD solvation model (solvent = water),[61] and frequency calculations were performed to verify the absence of negative vibrational frequencies. Counterions were not included in the calculations, under the assumption that ion pairing should be negligible in water. The pK_a values were estimated by comparing the computed free energies of the protonated and deprotonated compounds in each case. Because pK_a = $\Delta G°$(deprotonation)/2.303RT, the free energy of deprotonation must be calculated [$\Delta G°$(deprotonation) = $\Delta G°$(solv,A$^-$) + $\Delta G°$(solv,H$^+$) − $\Delta G°$(solv,HA) for an acid HA]. The difficulty in calculating pK_a values is that an accurate value for the standard free energy of the solvation of a proton in water, $\Delta G°$(solv,H$^+$), is needed. Because the pK_a of 2-hydroxypyridine is known (11.62), identical computational methods were used to back-calculate a value for $\Delta G°$(solv,H$^+$) as −283.2 kcal mol^{-1}, and this value was added to the calculated differences in energy between the deprotonated and protonated forms of the complexes reported herein to obtain estimates of their pK_a values. Similar methods of pK_a calculations have been previously described.[62]

DLS. A 10 mL solution of precatalyst (136.4 μM) in a pH 6.0, 180 mM aqueous acetate buffer was added to a vial containing NaIO$_4$ (0.021g, 0.09818 mmol), resulting in a final NaIO$_4$ concentration of 10 mM. The solution was allowed to mix, and NaIO$_4$ was completely dissolved within 1 min. After 20 min of reaction time, ~1.5 mL of the sample was transferred to a clear disposable particle size measurement cell (DTS0012, Malvern Instruments, Ltd.), equilibrated at 25 °C for 60 s, and then measured on a Zetasizer Nano ZS instrument (manufacturer: Malvern Instruments, Ltd.) equipped with a 50 mW, 633 nm laser with scattered light being detected at 173° to the direction of the incident light (173° backscatter NIBS default), which is an optimal geometry for detecting small particles. Each solution was analyzed at least three times.

ASSOCIATED CONTENT

Ⓢ Supporting Information

Further experimental details, methods, and characterization data relevant to the synthesis of ligands and known complexes, thermodynamic acidity measurements, water oxidation experiments, DLS, mechanistic studies, electrochemistry experiments (CV), computational methods and resulting *xyz* coordinates, and crystallographic data for **2** and **5** in CIF format. This material is available free of charge via the Internet at http://

pubs.acs.org. The atomic coordinates for these structures have also been deposited with the Cambridge Crystallographic Data Centre as CCDC 909508−909509. The coordinates can be obtained, upon request, from the Director, Cambridge Crystallographic Data Centre, 12 Union Road, Cambridge CB2 1EZ, U.K.

AUTHOR INFORMATION

Corresponding Author

*E-mail: jared.paul@villanova.edu (J.J.P.), elizabeth.papish@drexel.edu (E.T.P.).

Author Contributions

‡The first two authors contributed equally to this work.

Notes

The authors declare no competing financial interest.

REFERENCES

(1) Lewis, N. S.; Nocera, D. G. *Proc. Natl. Acad. Sci.* **2006**, *103*, 15729−15735.

(2) Concepcion, J. J.; Jurss, J. W.; Brennaman, M. K.; Hoertz, P. G.; Patrocinio, A. O. T.; Murakami Iha, N. Y.; Templeton, J. L.; Meyer, T. J. *Acc. Chem. Res.* **2009**, *42*, 1954−1965.

(3) Blakemore, J. D.; Schley, N. D.; Balcells, D.; Hull, J. F.; Olack, G. W.; Incarvito, C. D.; Eisenstein, O.; Brudvig, G. W.; Crabtree, R. H. *J. Am. Chem. Soc.* **2010**, *132*, 16017−16029.

(4) McDaniel, N. D.; Coughlin, F. J.; Tinker, L. L.; Bernhard, S. *J. Am. Chem. Soc.* **2008**, *130*, 210−217.

(5) Dismukes, G. C.; Brimblecombe, R.; Felton, G. A. N.; Pryadun, R. S.; Sheats, J. E.; Spiccia, L.; Swiegers, G. F. *Acc. Chem. Res.* **2009**, *42*, 1935−1943.

(6) Ellis, W. C.; McDaniel, N. D.; Bernhard, S.; Collins, T. J. *J. Am. Chem. Soc.* **2010**, *132*, 10990−10991.

(7) Fillol, J. L.; Codolà, Z.; Garcia-Bosch, I.; Gómez, L.; Pla, J. J.; Costas, M. *Nat. Chem.* **2011**, *3*, 807−813.

(8) Lutterman, D. A.; Surendranath, Y.; Nocera, D. G. *J. Am. Chem. Soc.* **2009**, *131*, 3838−3839.

(9) Gerken, J. B.; McAlpin, J. G.; Chen, J. Y. C.; Rigsby, M. L.; Casey, W. H.; Britt, R. D.; Stahl, S. S. *J. Am. Chem. Soc.* **2011**, *133*, 14431−14442.

(10) Dogutan, D. K.; McGuire, R., Jr.; Nocera, D. G. *J. Am. Chem. Soc.* **2011**, *133*, 9178−9180.

(11) McAlpin, J. G.; Stich, T. A.; Ohlin, C. A.; Surendranath, Y.; Nocera, D. G.; Casey, W. H.; Britt, R. D. *J. Am. Chem. Soc.* **2011**, *133*, 15444−15452.

(12) Concepcion, J. J.; Harrison, D. P.; Ashford, D. L.; Norris, M. R.; Binstead, R. A.; Luo, H.; Templeton, J. L.; Meyer, T. J. Conference Proceedings from the 243rd National Meeting of the American Chemical Society, 2012; INOR-627.

(13) Barnett, S. M.; Goldberg, K. I.; Mayer, J. M. *Nat. Chem.* **2012**, 498−502.

(14) Umena, Y.; Kawakami, K.; Shen, J.-R.; Kamiya, N. *Nature* **2011**, *473*, 55−60.

(15) Rakowski Dubois, M.; Dubois, D. L. *Chem. Soc. Rev.* **2008**, *38*, 62−72.

(16) Himeda, Y.; Onozawa-Komatsuzaki, N.; Sugihara, H.; Kasuga, K. *Organometallics* **2007**, *26*, 702−712.

(17) Himeda, Y. *Eur. J. Inorg. Chem.* **2007**, *2007*, 3927−3941.

(18) Hashiguchi, B. G.; Young, K. J. H.; Yousufuddin, M.; Goddard, W. A., III; Periana, R. A. *J. Am. Chem. Soc.* **2010**, *132*, 12542−12545.

(19) Crabtree, R. H. *Science* **2010**, *330*, 455−456.

(20) Noyori, R.; Sandoval, C. A.; Muñiz, K.; Ohkuma, T. *Philos. Trans. R. Soc., A* **2005**, *363*, 901−912.

(21) Duan, L.; Fischer, A.; Xu, Y.; Sun, L. *J. Am. Chem. Soc.* **2009**, *131*, 10397−10399.

(22) Privalov, T.; Åkermark, B.; Sun, L. *Chem.—Eur. J.* **2011**, *17*, 8313−8317.

(23) Klein, S.; Dougherty, W. G.; Kassel, W. S.; Dudley, T. J.; Paul, J. J. *Inorg. Chem.* **2011**, *50*, 2754−2763.

(24) Liu, F.; Concepcion, J. J.; Jurss, J. W.; Cardolaccia, T.; Templeton, J. L.; Meyer, T. J. *Inorg. Chem.* **2008**, *47*, 1727−1752.

(25) Nieto, I.; Livings, M. S.; Sacci, J. B. I.; Reuther, L. E.; Zeller, M.; Papish, E. T. *Organometallics* **2011**, *30*, 6339−6342.

(26) Conifer, C. M.; Taylor, R. A.; Law, D. J.; Sunley, G. J.; White, A. J. P.; Britovsek, G. J. P. *Dalton Trans.* **2011**, *40*, 1031−1033.

(27) Kawahara, R.; Fujita, K.-I.; Yamaguchi, R. *J. Am. Chem. Soc.* **2012**, *134*, 3643−3646.

(28) Li, H.; Jiang, J.; Lu, G.; Huang, F.; Wang, Z.-X. *Organometallics* **2011**, *30*, 3131−3141.

(29) Fujita, K.-I.; Tanino, N.; Yamaguchi, R. *Org. Lett.* **2007**, *9*, 109−111.

(30) Hull, J. F.; Himeda, Y.; Wang, W.-H.; Hashiguchi, B.; Periana, R.; Szalda, D. J.; Muckerman, J. T.; Fujita, E. *Nat. Chem.* **2012**, *4*, 383−388.

(31) Wang, W.-H.; Hull, J. F.; Muckerman, J. T.; Fujita, E.; Himeda, Y. *Energy Environ. Sci.* **2012**, *5*, 7923.

(32) Dubreuil, D. M.; Pipelier, M. G.; Pradere, J. P.; Bakkali, H.; Lepape, P.; Delaunay, T.; Tabatchnik, A. (CNRS, France). Pyridazine and pyrrole compounds, processes for obtaining them and uses. World Patent 012440A2, 2008.

(33) Umemoto, T.; Nagayoshi, M.; Adachi, K.; Tomizawa, G. *J. Org. Chem.* **1998**, *63*, 3379−3385.

(34) Jeffrey, G. A. *Crystallogr. Rev.* **2003**, *9*, 135−176.

(35) Schwederski, B.; Kaim, W. *Inorg. Chim. Acta* **1992**, *195*, 123−126.

(36) Pallavicini, P. S.; Perotti, A.; Poggi, A.; Seghi, B.; Fabbrizzi, L. *J. Am. Chem. Soc.* **1987**, *109*, 5139−5144.

(37) Wu, L.; Shen, X.-M.; Liu, D. Q. *J. Pharm. Biomed. Anal.* **2008**, *48*, 8−12.

(38) Hong, D.; Murakami, M.; Yamada, Y.; Fukuzumi, S. *Energy Environ. Sci.* **2012**, *5*, 5708−5716.

(39) Nair, V.; Deepthi, A. *Chem. Rev.* **2007**, *107*, 1862−1891.

(40) Schley, N. D.; Blakemore, J. D.; Subbaiyan, N. K.; Incarvito, C. D.; D'Souza, F.; Crabtree, R. H.; Brudvig, G. W. *J. Am. Chem. Soc.* **2011**, *133*, 10473−10481.

(41) Blakemore, J. D.; Schley, N. D.; Olack, G. W.; Incarvito, C. D.; Brudvig, G. W.; Crabtree, R. H. *Chem. Sci.* **2010**, *2*, 94−98.

(42) Grotjahn, D. B.; Brown, D. B.; Martin, J. K.; Marelius, D. C.; Abadjian, M.-C.; Tran, H. N.; Kalyuzhny, G.; Vecchio, K. S.; Specht, Z. G.; Cortes-Llamas, S. A.; Miranda-Soto, V.; van Niekerk, C.; Moore, C. E.; Rheingold, A. L. *J. Am. Chem. Soc.* **2011**, *133*, 19024−19027.

(43) Stracke, J. J.; Finke, R. G. *J. Am. Chem. Soc.* **2011**, *133*, 14872.

(44) Weiner, H.; Hayashi, Y.; Finke, R. G. *Inorg. Chem.* **1999**, *38*, 2579.

(45) Mondloch, J. E.; Bayram, E.; Finke, R. G. *J. Mol. Catal., A: Chem.* **2012**, *355*, 1.

(46) Parent, A. R.; Blakemore, J. D.; Brudvig, G. W.; Crabtree, R. H. *Chem. Commun.* **2011**, *47*, 11745−11747.

(47) Parent, A. R.; Brewster, T. P.; De Wolf, W.; Crabtree, R. H.; Brudvig, G. W. *Inorg. Chem.* **2012**, *51*, 6147−6152.

(48) Kaszuba, M.; McKnight, D.; Connah, M. T.; McNeil-Watson, F. K.; Nobbmann, U. *J. Nanopart. Res.* **2008**, *10*, 823−829.

(49) Fuentes, M. J.; Bognanno, R. J.; Dougherty, W. G.; Boyko, W. J.; Kassel, W. S.; Dudley, T. J.; Paul, J. J. *Dalton Trans.* **2012**, *41*, 12514−12523.

(50) Preliminary studies with 6,6′-dhbp suggest that no oxidation events occur within the solvent window for the neutral ligand in trifluoroethanol, and when the ligand is doubly deprotonated (in CH_3CN and water), it oxidizes at 0.65 V vs SCE. However, it appears that the ligand (in both the neutral and deprotonated forms) forms strong metal complexes and should be less vulnerable to oxidation when coordinated to a metal.

(51) Pecht, I.; Luz, Z. *J. Am. Chem. Soc.* **1965**, *87*, 4068−4072.

(52) Rappaport, F.; Lavergne, J. *Biochemistry* **1991**, *30*, 10004−10012.

(53) Takashima, T.; Hashimoto, K.; Nakamura, R. *J. Am. Chem. Soc.* **2012**, *134*, 1519−1527.

(54) Brewster, T. P.; Blakemore, J. D.; Schley, N. D.; Incarvito, C. D.; Hazari, N.; Brudvig, G. W.; Crabtree, R. H. *Organometallics* **2011**, *30*, 965−973.

(55) Youinou, M.-T.; Ziessel, R. *J. Organomet. Chem.* **1989**, *363*, 197−208.

(56) Frisch, M. J. et al. *Gaussian09*, revision A.02; Gaussian, Inc.: Wallingford, CT, 2004.

(57) Becke, A. D. *J. Chem. Phys.* **1993**, *98*, 5648−5652.

(58) Lee, C.; Yang, W.; Parr, R. G. *Phys. Rev. B* **1988**, *37*, 785−789.

(59) (a) Hehre, W. J.; Ditchfield, R.; Pople, J. A. *J. Chem. Phys.* **1972**, *56*, 2257−2261. (b) Hariharan, P. C.; Pople, J. A. *Theor. Chem. Acc.* **1973**, *28*, 213−222. (c) Ehlers, A. W.; Böhme, M.; Dapprich, S.; Gobbi, A.; Höllwarth, A.; Jonas, V.; Köhler, K. F.; Stegmann, R.; Veldkamp, A.; Frenking, G. *Chem. Phys. Lett.* **1993**, *208*, 111−114. (d) Höllwarth, A.; Böhme, M.; Dapprich, S.; Ehlers, A. W.; Gobbie, A.; Jonas, V.; Köhler, K. F.; Stegmann, R.; Veldkamp, A.; Frenking, G. *Chem. Phys. Lett.* **1993**, *203*, 237−240.

(60) (a) Andrae, D.; Häussermann, U.; Dolg, M.; Stoll, H.; Preuss, H. *Theor. Chim. Acta* **1990**, *77*, 123−141. (b) Bergner, A.; Dolg, M.; Küchle, W.; Stoll, H.; Preuss, H. *Mol. Phys.* **1993**, *30*, 1431−1441.

(61) Marenich, A. V.; Cramer, C. J.; Truhlar, D. G. *J. Phys. Chem. B* **2009**, *113*, 6378−6396.

(62) (a) Jang, Y. H.; Goddard, W. A., III; Noyes, K. T.; Sowers, L. C.; Hwang, S.; Chung, D. S. *J. Phys. Chem. B* **2003**, *107*, 344−357. (b) Surawatanawong, P.; Tye, J. W.; Darensbourg, M. Y.; Hall, M. B. *Dalton Trans.* **2010**, *39*, 3093−3104.